REQ. NO. 3-9130

CONTRACT REPORT NO. OSU83-00121

Department of Metallurgy and Materials Science
McMaster University
Hamilton, Ontario, Canada

Final Report on

THE DEVELOPMENT OF NON-DESTRUCTIVE TESTING TECHNIQUES FOR THE EVALUATION OF SINTERED SOLID ELECTROLYTES - PHASE III

Patrick S. Nicholson

Research Associates: N.D. Patel
A. Stockman
J. van den Andel

Research Contract File #DSS 14SU.23440-3-9130

For

Dr. T. Wheat
CANMET, EMR
Ottawa, Ontario, Canada

OCT 26 1984

MICROMEDIA

June 1984

35 pp

EXECUTIVE SUMMARY

This report is concerned with the development of techniques of identifying defects in high performance ceramics non-destructively using ultrasound. Since ceramic component performance is degraded by even the smallest of flaws it is important to identify these components which might fail during normal operation. Ultrasound is a technique which can "see" into materials using sound waves; however, to detect very small defects, high frequency sound must be used. Transducers which produce sound in the frequency and power ranges which can penetrate the components are difficult to manufacture for many reasons. Some of these reasons are examined herein along with a report on the progress and success in overcoming them.

Sommaire

Ce rapport concerne le développement de techniques ultrasoniques afin de détecter, puis d'identifier des défauts dans des céramiques à hautes performances mécaniques; ce de maniére non destructive.

Comme les performances de ces composants céramiques se dégradent rapidementen présence du plus petit des défauts; il est important de les détecter d'une maniére fiable.

Les ultrasons sont une technique qui permet réellement de "voir" á travers les matériaux par l'intermédiaire d'ondes soniques; et donc de détecter des défauts de toutes tailles.

Cependant la taille du défaut détecté est inversement proportionnelle à la fréquence et la puissance sonique utilisées. Les "transducers" qui permettent l'obtention de hautes fréquences (pour les micro-défauts), susceptibles de pénétrer ces céramiques sont d'une facture complexe pour de nombreuses raisons.

Ces raisons seront examinées et discutées tout au long de ce rapport et un certain nombres de solutions seront proposees quant à la synthése de ces "transducers".

I INTRODUCTION

This is the final report for FY 1983-84. It is divided into the natural subdivisions associated with the work in progress. Equipment development is dealt with first, followed by a discussion of the use of the equipment to analyze defects. From this work, clear shortcomings in the available transducers become evident and the development of crystals for transducers and the transducers themselves is discussed in the last section.

II PROGRESS IN FACILITY DEVELOPMENT

During this FY, new equipment was purchased via grants from the Ontario and Federal Governments. This equipment was set up as per block diagrams (Figs. 1, 2 and 3) and these configurations were used to compare the capabilities of the Panametric and Matec ultrasonic equipment. It is clear from the time-signal spectra (Figures 4-7) that the Matec improves our capabilities of detecting low level signals from small defects, i.e., the signal to noise ratio increased with the system set up in Figure 3. This results from using the Matec system or Matec pre-amplifier in conjunction with the Panametric pulser. The main advantages of the Matec System are:

1) the increased power output
2) the control of the pulse length either in a step of ten cycles (see Figure 7) or varying continuously
3) both rf and video pulses can be obtained
4) it can be tuned to the frequency for optimum output
5) the c.w. source of the Matec system can be used for measuring the coupling coefficient of a piezo-electric ceramic

Figures 4 through 7 were generated on the PDP 11/23 computer with data

obtained from a Tektronix 7612D Transient Digitizer. Programs were written to allow the system to require waveforms of back-reflected signals, then select a section for analysis . In this instance (Figures 4-7) the back-reflected signal from a void in glass was selected. This selected region has been Fourier transformed to obtain the frequency spectrum necessary to size the defect. Although not used in this example, it is possible to signal-average the defect signal to remove the effects of noise and thereby analyze defects previously observed only by visual inspection.

The scanner was completed very early in the FY. Some fine adjustments were made later. Upon receiving the motor control, the scanner was wired and limit switches installed. Problems with the control are well documented, but in order to continue the research program, the old, low power scanner control was augmented with a power stage to enable us to scan small samples albeit slowly (18 hours per scan). This was in part due to the inability of the old control to communicate with the computer. Instead, the ultrasonic signals were digitized, sorted by the computer and stored in the memory. Five steps per second was the maximum scan rate of the X-driving stepper motor.

III PROGRESS IN DEVELOPMENT OF HIGH FREQUENCY TRANSDUCERS

The production of dense, fine-grained ceramic crystals is vital to high-frequency transducer development. To this end, a split molybdenum-mold system was designed and made to hot press PZT materials in a vacuum induction furnace. This design ensures easy removal of the hot pressed PZT specimen. After a series of temperature, time and external pressure experiments, the best conditions for hot pressing PZT materials were found. These were 1100 $\pm$10^{o}C at 35 MPa (5000 $\pm$100 psi) of external pressure for 150-180 minutes. These conditions give ~100% dense material. The covering powder plays a vital role in the densification of

these PZT materials. A blanket of fine ZrO_2 powder gave the best results. Figure 8 shows the densification of a PZT 5 composition from 800°C to 1100°C at 7-35 MPa from 5 min. to 240 min. Analysis of the data as a function of time revealed that densification is diffusion controlled.

As these materials were pressed in vacuum, there was a loss of oxygen. Therefore, a series of heat-treatment cycles in air were performed to reoxidize them. For PZT 5, a temperature of 1250°C in a controlled atmosphere gave the best results. The hot-pressed results are compared with those for sintered and commercial materials in Table I.

The planar coupling coefficient k_p, which is a function of composition, density and dielectric constant, is also dependent on poling conditions. Therefore, optimum poling conditions were identified for each PZT composition. Figures 9 and 10 show these data at a constant poling temperature of 120°C for PZT 7 and PZT 4, at 145°C for PZT 5 composition. In the course of poling, the dipole alignment caused by the application of the electric field contributes to the development of internal stress. If the poling condition (i.e., poling field, time and temperature) exceeds the optimum condition, the k_p decreases. This behaviour under severe poling conditions is postulated to be due to slow crack growth along grain boundaries (Ref.1). This is supported by the fluctuation and increase in dissipation current during poling (Figures 11 and 12) for sintered and hot pressed elements.

In assembling a transducer, wire is either soldered to the electrode of the element, (Indium bonding (160°C)) or conducting epoxy is used (normally cures at high temperature). In either case, the piezoelectric elements are heated up. In order to examine the effect of temperature on the piezoelectric properties, the frequency of maximum and minimum impedance were measured as a function of temperature and the coupling coefficients calculated (Figure 13). After each

heat treatment (i.e., up to 200°C), the coupling coefficient was measured at room temperature and was found to be lower than the initial value when the temperature exceeded 110°C. In Figure 14, the planar coupling coefficient is shown for a heating/cooling cycle to 175°C. Up to 110°C, the planar coupling coefficient increased with temperature, but then returned to its original room temperature value. This effect will now be further discussed.

There is a strong dependence of longitudinal modulus with the degree of polarisation when measured along the thickness. The sound velocity (which controls the thickness resonance frequency) increases with the degree of polarisation. In order to understand the mechanism of polarisation, it was decided to polarise hot pressed PZT 5 in a different field and then depolarise this specimen at a different temperature. Figure 15 shows the data measured on 2 hot pressed and 2 sintered PZT 5 elements. For PZT 5 materials, 31-40% K_p values are obtained via alignment of the 180° dipoles. These dipoles are easily aligned with very low fields since no structural changes are associated therewith. However, for dipoles other than 180°, structural changes must occur during poling (i.e., alignment of dipoles along the direction of field). This will affect the interatomic forces, resulting in the observed increase in the compressional sound velocity along the polarisation direction. Depolarisation occurs via the switching back of other-than-180° dipoles (see Figure 15). As seen in Figure 15, hot pressed PZT 5 depolarised about 10% of its original value at 200°C. However, in the past, most PZT 5 materials would depolarise to < 50% of their original values at 200°C. From both longitudinal velocity and radial mode frequency measurements on polarised PZT 5, a 10% change in dimension (i.e., diameter increase and length decrease) is expected if the explanation of changing inter-atomic forces does not hold. However, the dimensions of these materials were not observed to change, therefore, velocity changes are due to

other-than-180° dipole alignment.

The hot pressed elements mentioned above did not suffer grain pull-outs during grinding and were used to develop high frequency transducers. Both planar and focussed transducers were constructed. The highest frequency achieved was 75 MHz for a planar transducer. The second backwall reflection from the 4 mm test steel specimen using the 75 MHz planar transducer is shown in Figures 16a and 16b. For focussed transducers, a maximum frequency of 56 MHz has been achieved. Figure 17a and Figure 17b show the reflected signal from a glass plate immersed in water using the 36 and 56 MHz focussed transducers.

Quartz lenses were obtained because their attenuation is much less than plastic lenses. They were difficult to thin down to the required thickness, therefore lenses of different materials will be experimented with.

A die was made to press aluminum lenses, which could be held in front of a transducer by means of a "holder" on the housing, i.e., an interchangeable lens system has been created. The aluminum doubles as the front electrode of the piezo-electric element. This technique is being developed.

Another die facilitates the manufacture of lenses of acrylic or other press-materials. This die can also be used to produce curved backings for the curved crystal development.

Equivalent circuits (Figure 18) with and without quarter wavelength matching sections of different backing materials have been solved. The plots of the transfer functions for transmitting and receiving circuits with a tungsten loaded epoxy backing are given in Figures 19-22.

The fundamental and overtone resonant frequencies of a thickness mode, piezoelectric resonator departs from the integral multiple relationship, when the electro-mechanical coupling of the resonator material becomes large. This can be verified by careful analysis of the free vibrations of a thickness-mode

piezoelectric resonator with short-circuited electrodes (Figure 23).

A computer program has been written, which calculates the circuit impedance of an undamped piezoelectric resonator. The equivalent circuit used is shown in Fig. 23. For selected materials with chosen relative dielectric constant, thickness, density, longitudinal speed of sound and electrode surface area, the program calculates the impedance for a user selected number of frequencies (f) and coupling coefficients (k_{33}) within the ranges specified by the user. The program takes the common log of the impedances and plots this against frequency and coupling coefficient. The solution for the equivalent circuit of Figure 23 is:

$$Z_t = j \frac{2\phi^2 \tan\alpha - Z_o \omega C_o}{(\omega C_o) Z_o}$$

where $\alpha = f/f_o$ $\quad f_o = \nu/t$ $\quad \phi = Ak_t/t(C_{33}^D \varepsilon_{33}^D)^{\frac{1}{2}}$

and C_o = clamped capacitance, A = area of resonator, t = thickness of resonator, C_{33}^D = elastic stiffness at constant charge density, ε_{33}^D = the clamped dielectric constant, ω = angular frequency, ν = the longitudinal sound velocity, and k_t = the electromechanical thickness coupling coefficient.

When the transducer is put in a circuit as shown in Figure 24, a maximum output voltage is obtained at a minimum value for Z_t. Thus, the relation $2\phi^2_{max} - \omega C_o Z_o$ determines the frequencies of circuital resonances from which k_t may be determined. Figures 25 and 26 show a sample output from the program. With the same procedure as above, one can obtain k_p values as well.

In summary, significant progress has been made in the area of quality ceramic fabrication. Transducers have been made using these crystals with encouraging results.

IV SUMMARY

During FY 1983-84, planar and focussed transducers of 75 MHz and 56 MHz

respectively, have been constructed. The heart of these developments is the improved grain-size/purity PZT piezoelectric ceramic discs that have been produced. Diligent use of equivalent circuits has helped to design transducers with increased bandwidth and higher power output.

REFERENCES

1. Chiang, S.S., Fulrath, R.M. and Pask, J.A., "Influence of Microcracking and Slow Crack Growth on the Planar Coupling Coefficient in PZT", Comm. of the Amer. Cer. Soc., C-141 (1981).

TABLE I

Comparison of piezoelectric, dielectric and elastic properties of commercial and McMaster-made piezoelectric elements

MATERIAL	DENSITY $kg/m^3 \times 10^3$	LONGITUDINAL VELOCITY m/sec	$\varepsilon_{33}^T/\varepsilon_o$	PLANAR COUPLING COEFFICIENT kp %	k_{31} %	d_{31} $\times 10^{-12}$ m/V	g_{31} $\times 10^{-3}$ V.m/N	θ_m	DISSIPATION FACTOR
PZT 4A COMMERCIAL	7.60	----	1250	58.0	33.0	-120	-10.5	650	0.35
SINTERED	7.74	4400	1200-1250	60.0	36.0	-(127-130)	-(11.7-11.9)	600	0.4
HOT PRESSED	7.99	4800	1280-1320	65.0	39.0	-(142-145)	-(12.4-12.5)	700	0.3
PZT 5A COMMERCIAL	7.70	----	2000	63.0	36.0	-175	-12.4	80	1.4
SINTERED	7.76	4000-4200	1300-1400	60-62.5	36-37	-(140-150)	-(12-13)	50	1.6
HOT PRESSED	8.07	4800-5000	2200-2400	70-72.5	41-43	-(190-230)	-(11-13)	70	1.45
MODIFIED AND HOT PRESSED	8.02	4800-5000	1800-2000	67-70	40-41	-(190-220)	-(12-13)	70	1.5
PZT 7 COMMERCIAL	7.30	----	550	28	16.5	-36	-8.5	1130	0.5
SINTERED	7.60	4600	500	32	18.9	-40	-9.0	1000	0.6
HOT PRESSED	8.00	5000	600	35	20.7	-49	-9.2	1100	0.5

BLOCK DIAGRAM 1

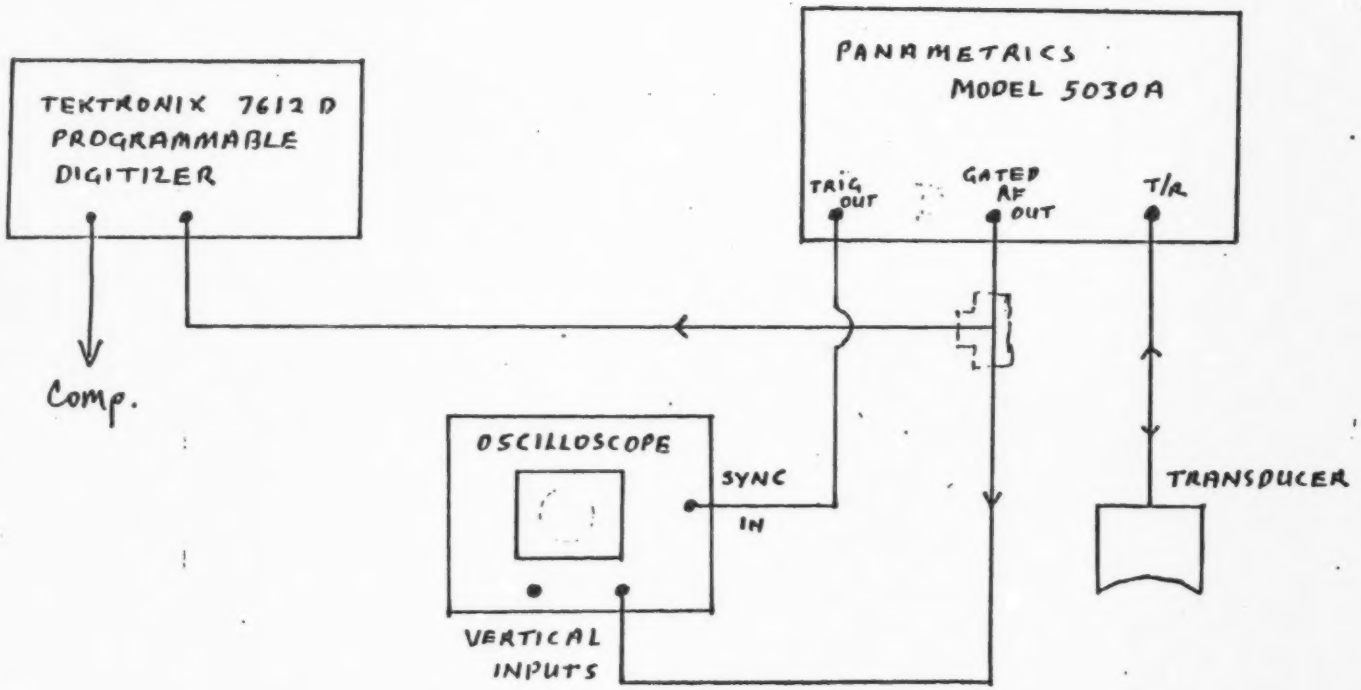

FIGURE 1

Block diagram of pulse echo method used for Ultrasonic testing. Transducer is excited by impulse method using Panametric pulser.

BLOCK DIAGRAM 2

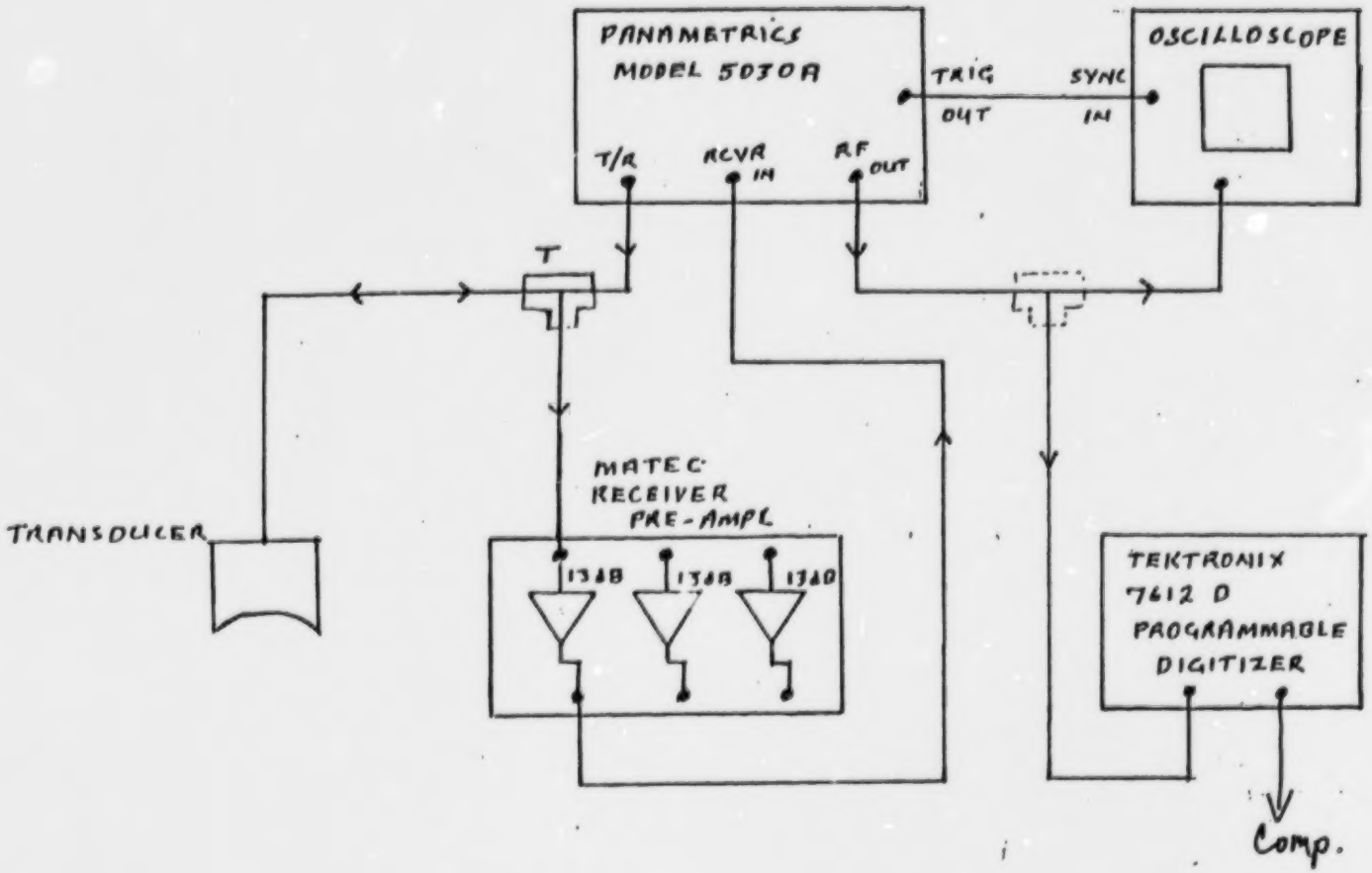

FIGURE 2

Block diagram of pulse echo method used for Ultrasonic testing. Transducer is excited by impulse method using Panametric pulser. Diagram includes the Matec preamplifier.

BLOCK DIAGRAM 3

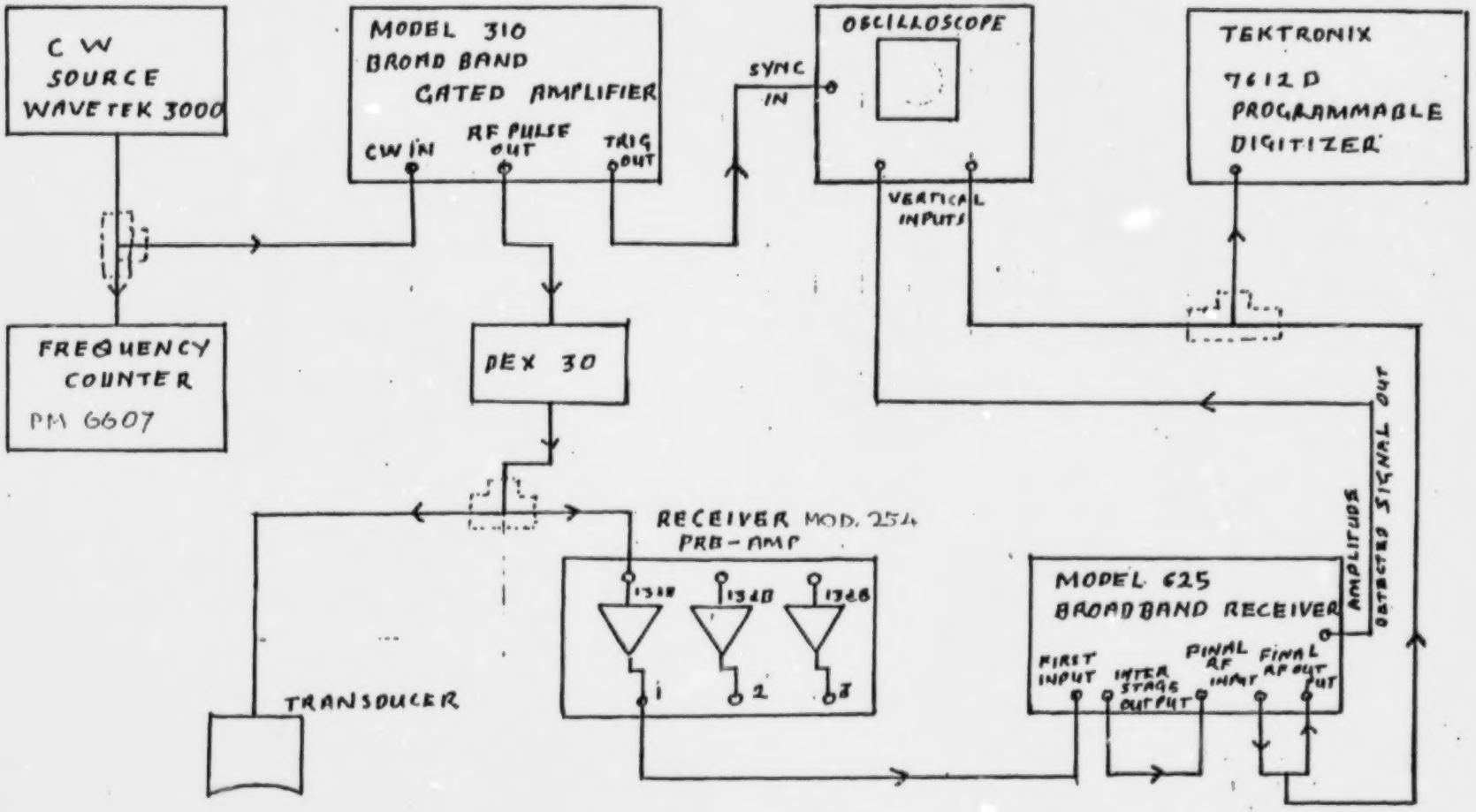

FIGURE 3

Block diagram of pulse echo method used for ultrasonic testing. Transducer is excited by tone burst method using Matec broad band system.

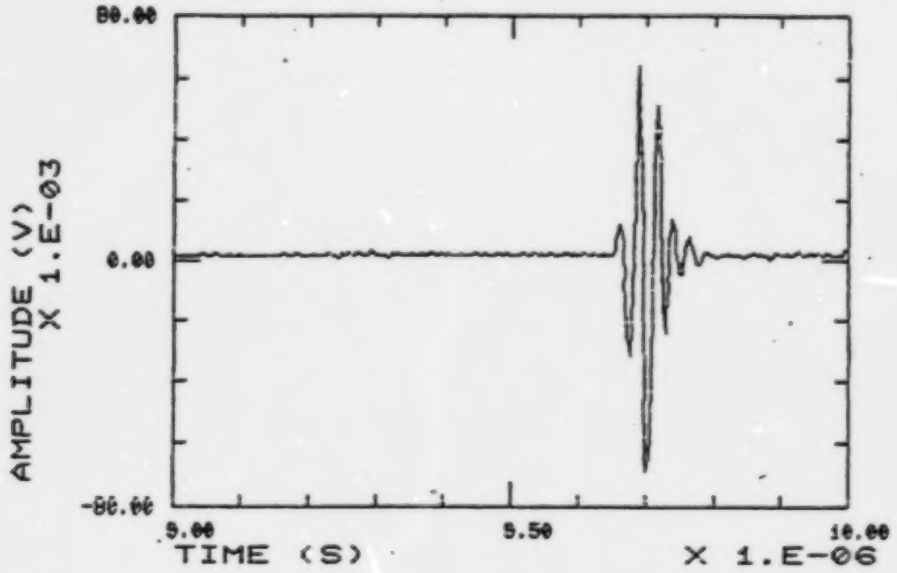

Peak to Peak - 145 mV.

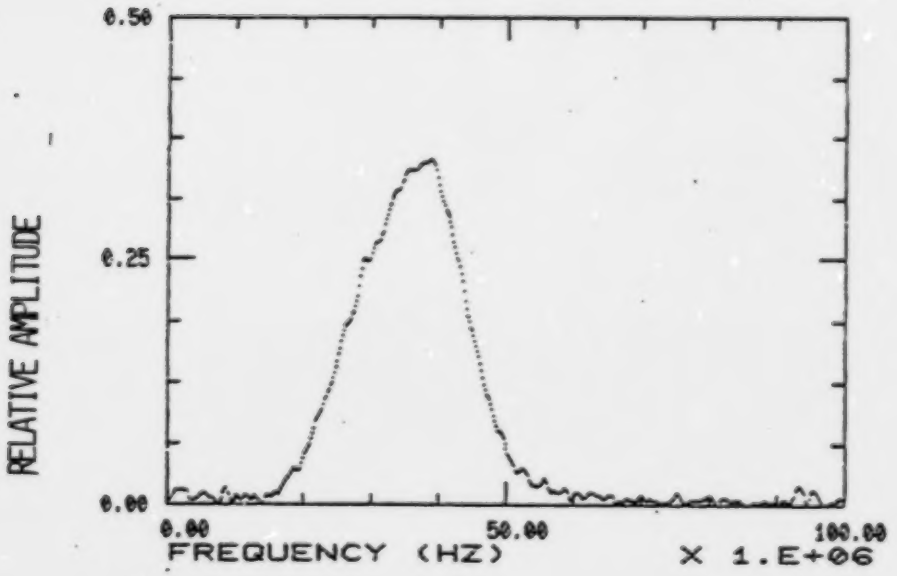

FIGURE 4

Time-signal spectra from ∿ 100 μm defect in a glass obtained using set-up shown in Fig. 1.

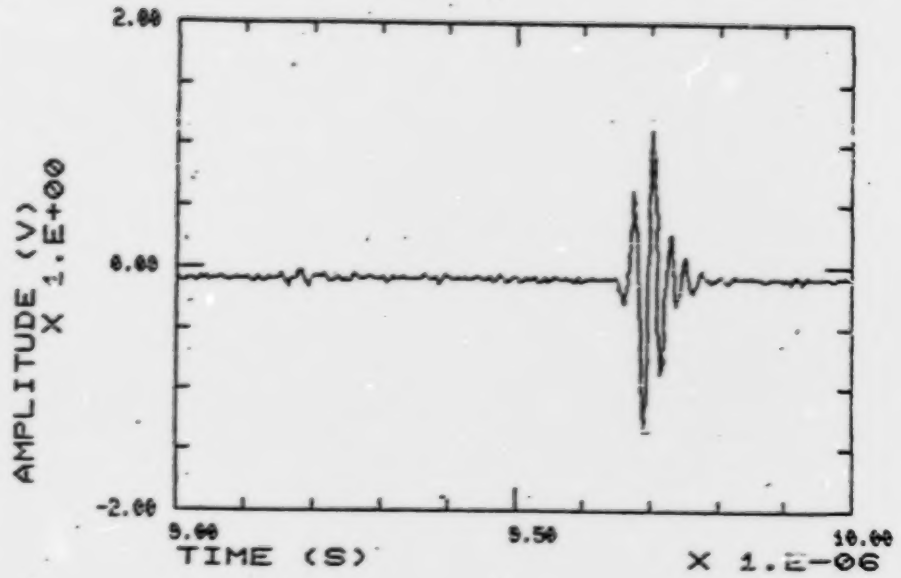

Peak to Peak - 3 volts

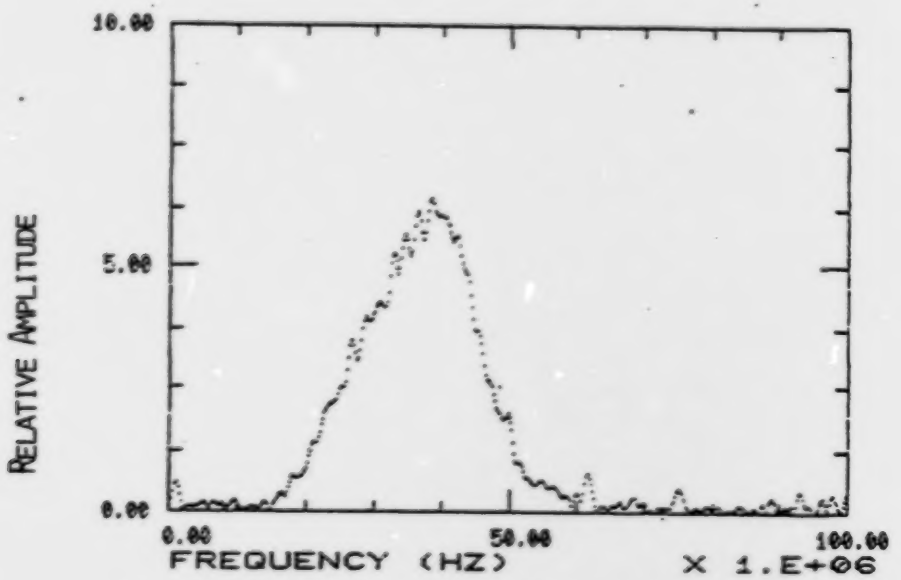

FIGURE 5

Time-signal spectra from ~ 100 μm defect in a glass obtained using set-up shown in Fig 2. There is moderate increase in signal to noise ratio (~ 6-10 dB) when compared with Fig. 4.

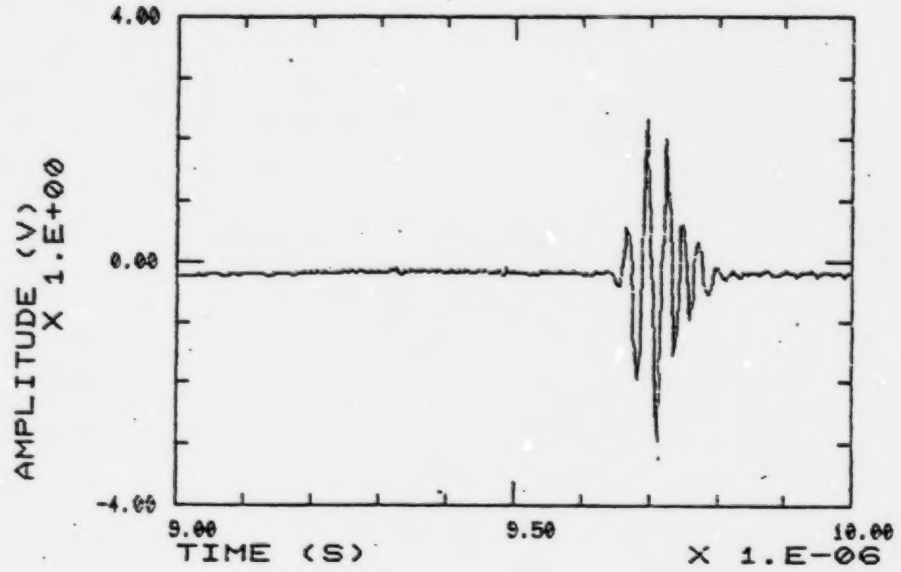

Peak to Peak - 5.5 volts

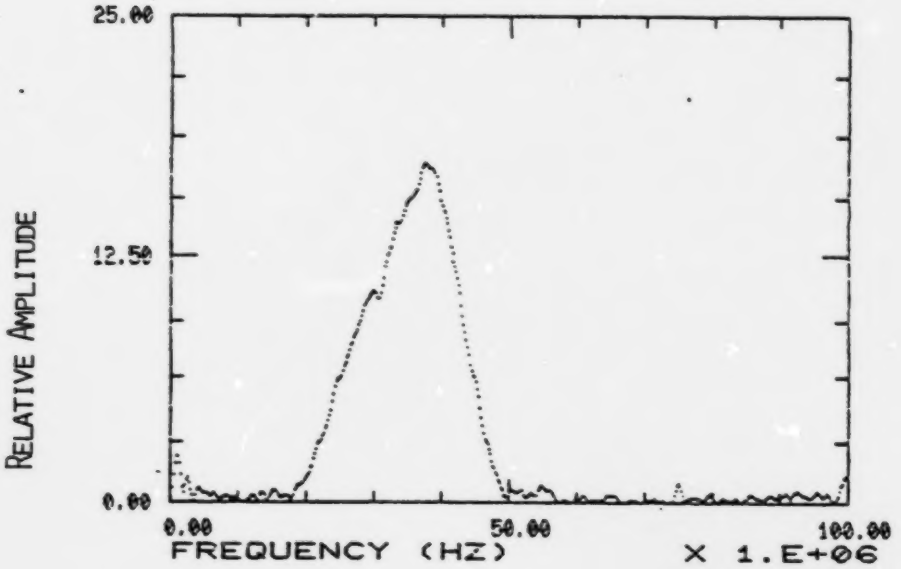

FIGURE 6

Time-signal spectra from ~ 100 μm defect in a glass obtained using set-up shown in Fig. 3. There is considerable increase in signal to noise ratio (15-18 dB) when compared with Fig. 4.

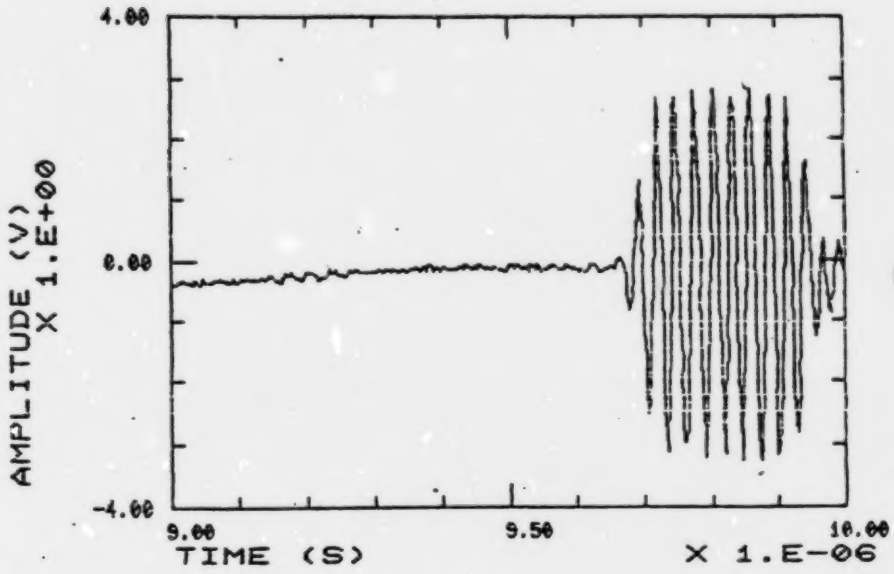

Peak to Peak - 6V.

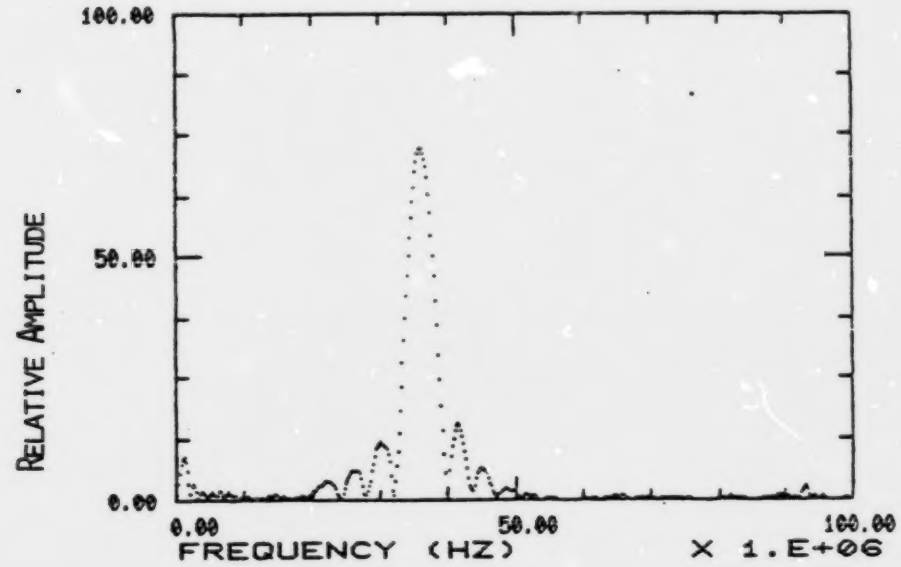

FIGURE 7

Time-signal spectra from ~ 100 μm defect in a glass obtained using set-up shown in Fig. 3. Excitation pulse width increased to 1 μs from < 0.5 μs.

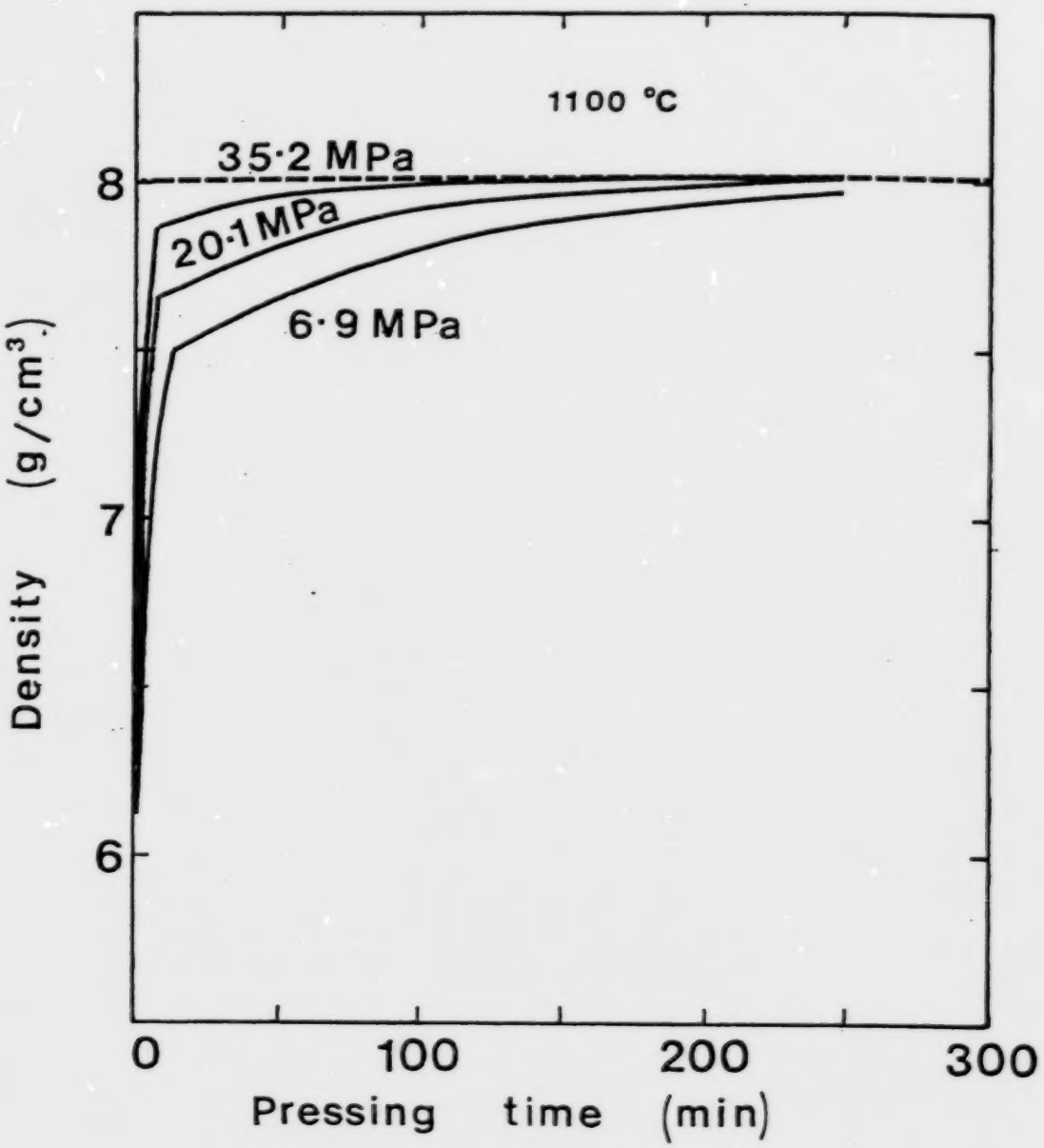

Figure 8: Variation of density as a function of time and pressure at constant temperature of 1100°C.

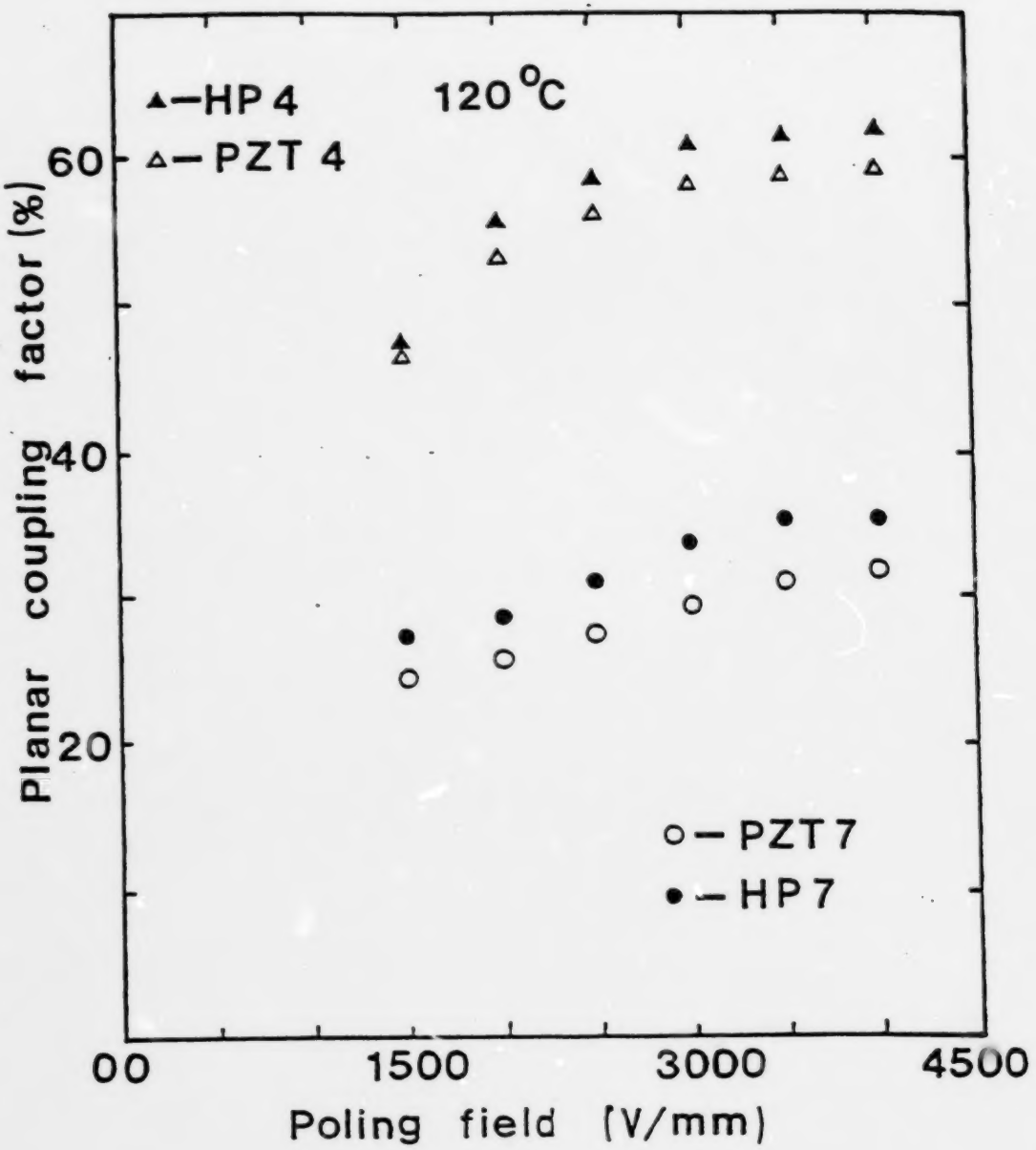

Figure 9: Planar coupling coefficient at a constant poling temperature of 120°C for PZT 7, HP7, PZT 4 and HP4

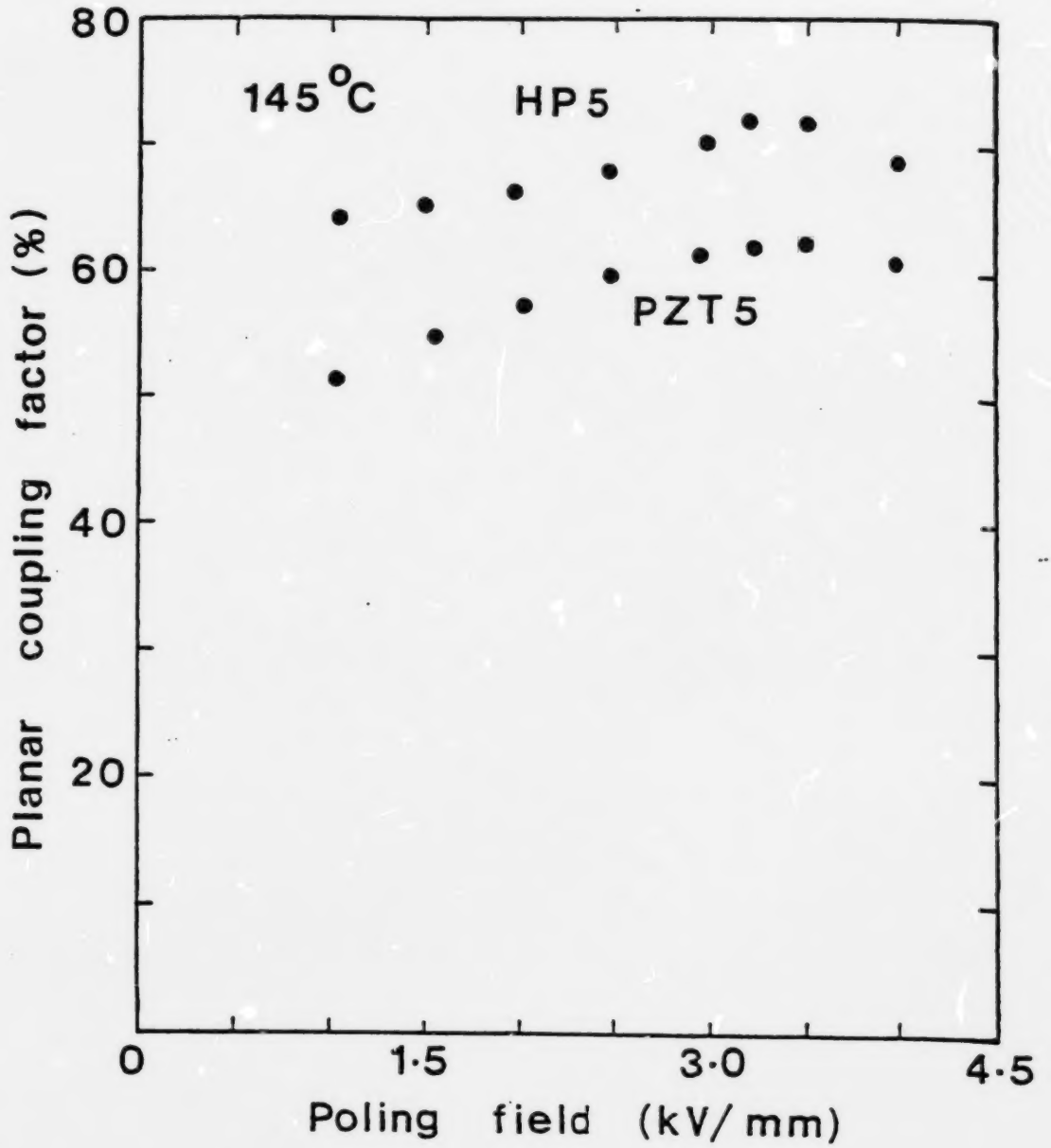

Figure 10: Planar coupling coefficient as a function of poling field at constant poling temperature of 145°C for PZT5 and HP5.

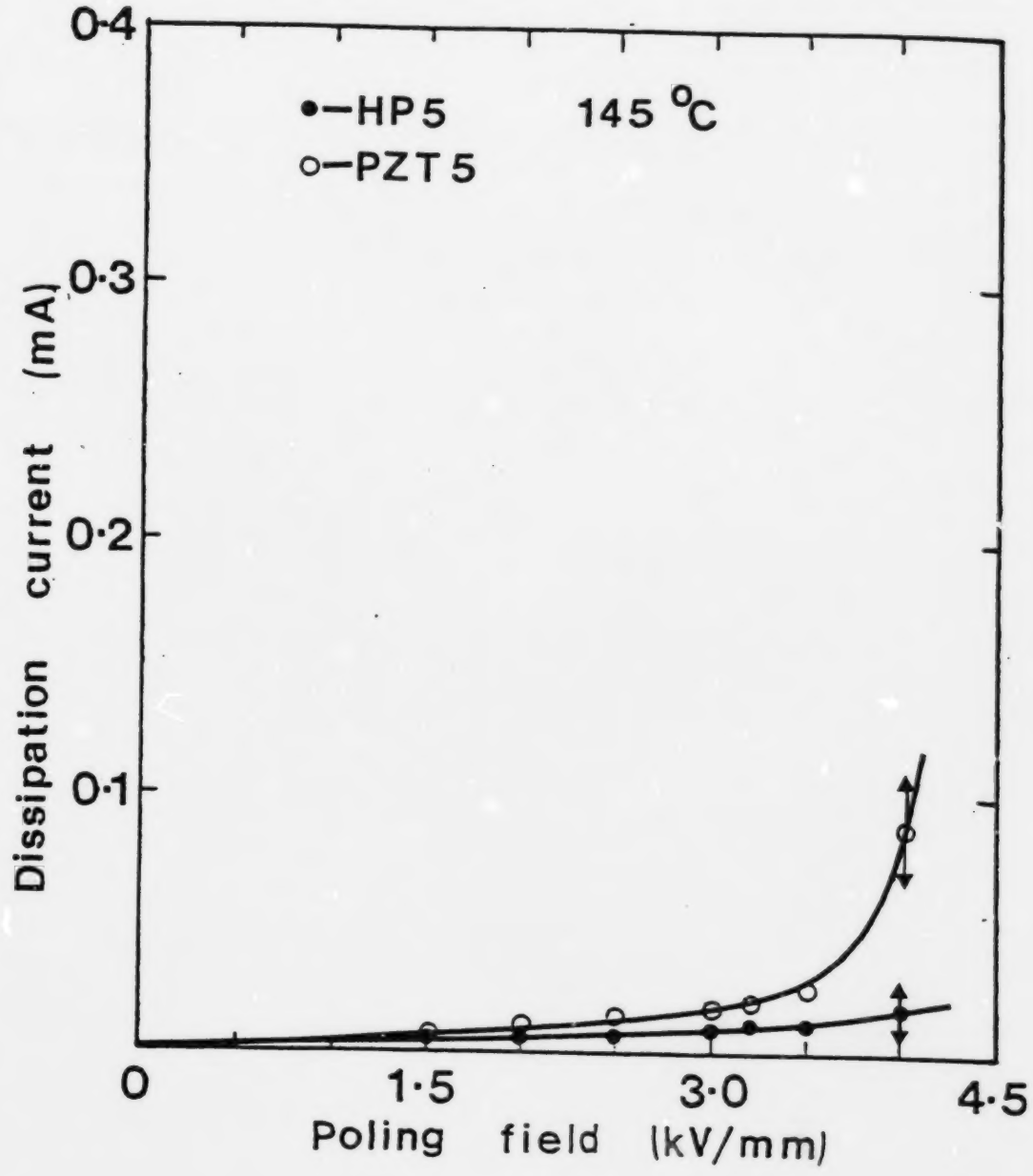

Figure 11: Dissipation current as a function of poling field at a constant poling temperature of 145°C for HP5(0) and PZT5.

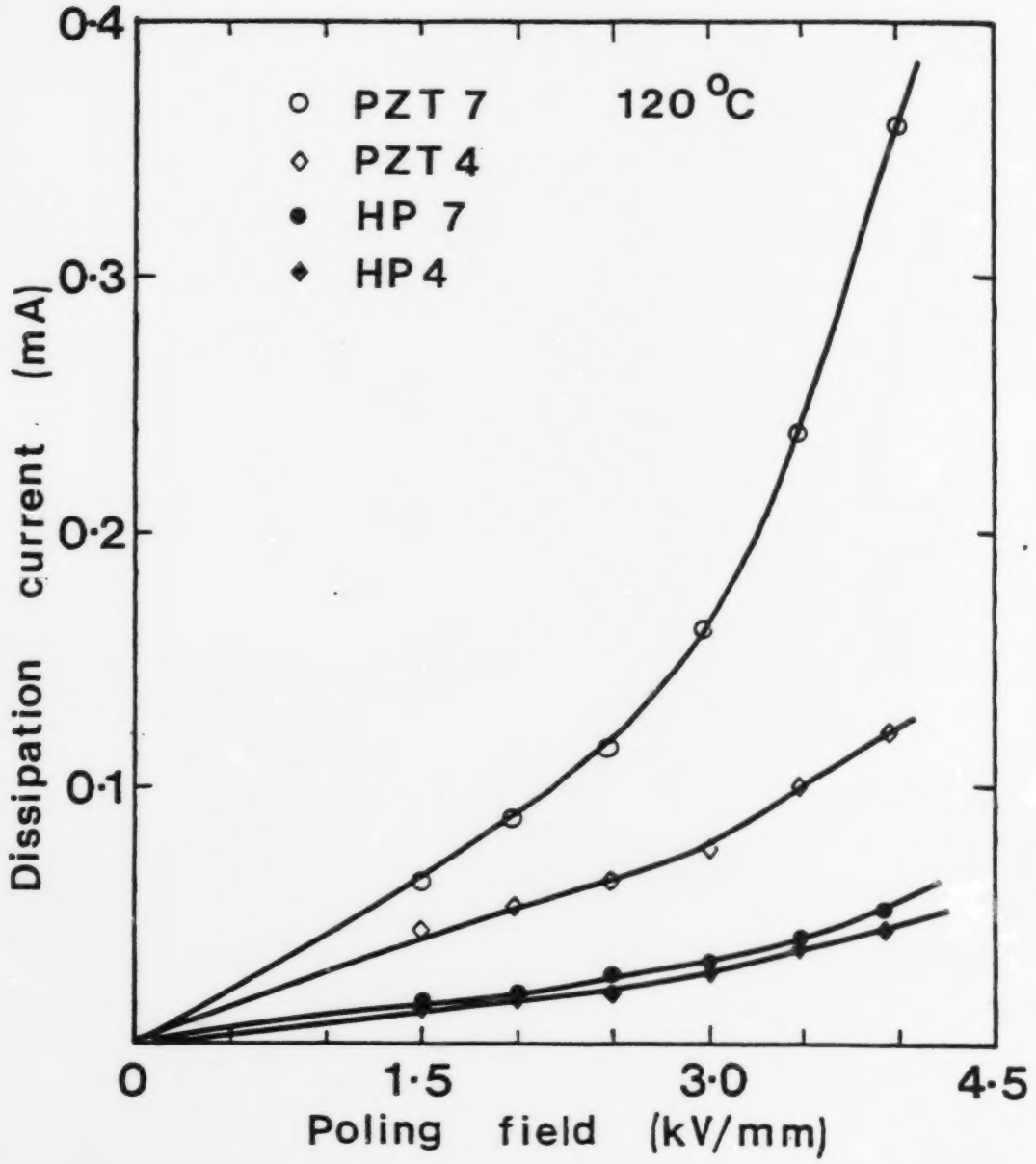

Figure 12: Dissipation current as a function of poling field at a constant poling temperature of 120°C, PZT4, HP7 and PZT7.

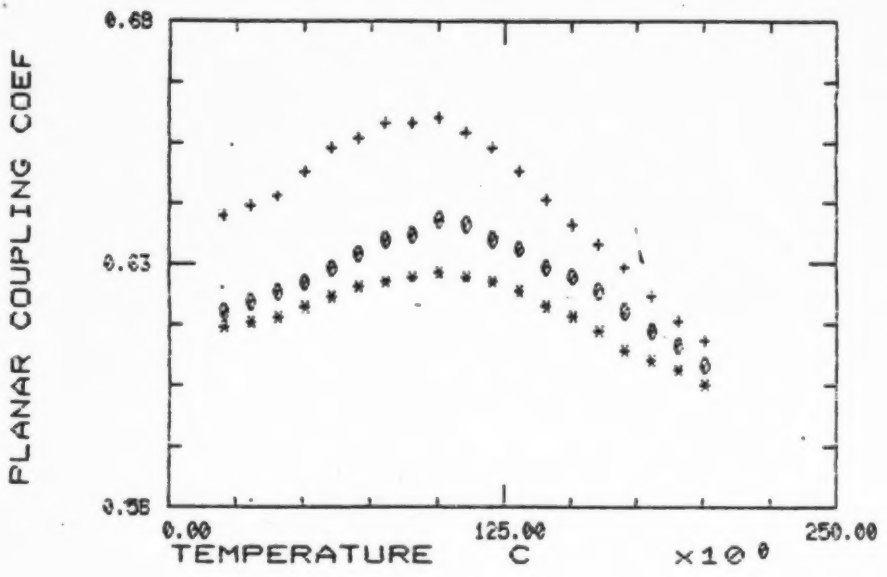

(+) 1st heat treatment cycle
(Ø) 2nd heat treatment cycle
(*) 3rd heat treatment cycle

Figure 13 The dependence of planar coupling coefficient on temperature for PZT5.

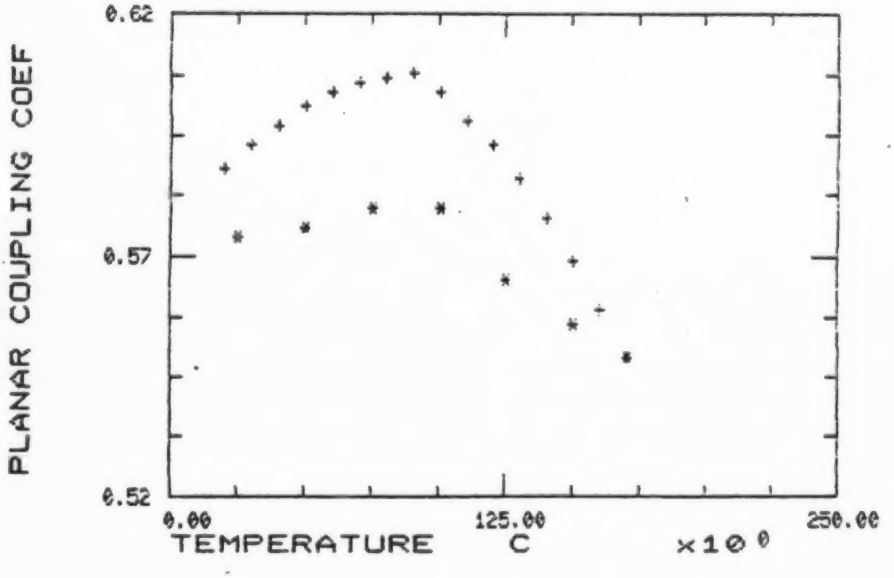

(+) heating
(*) cooling

Figure 14: The dependence of planar coupling coefficient on a temperature cycle for PZT5.

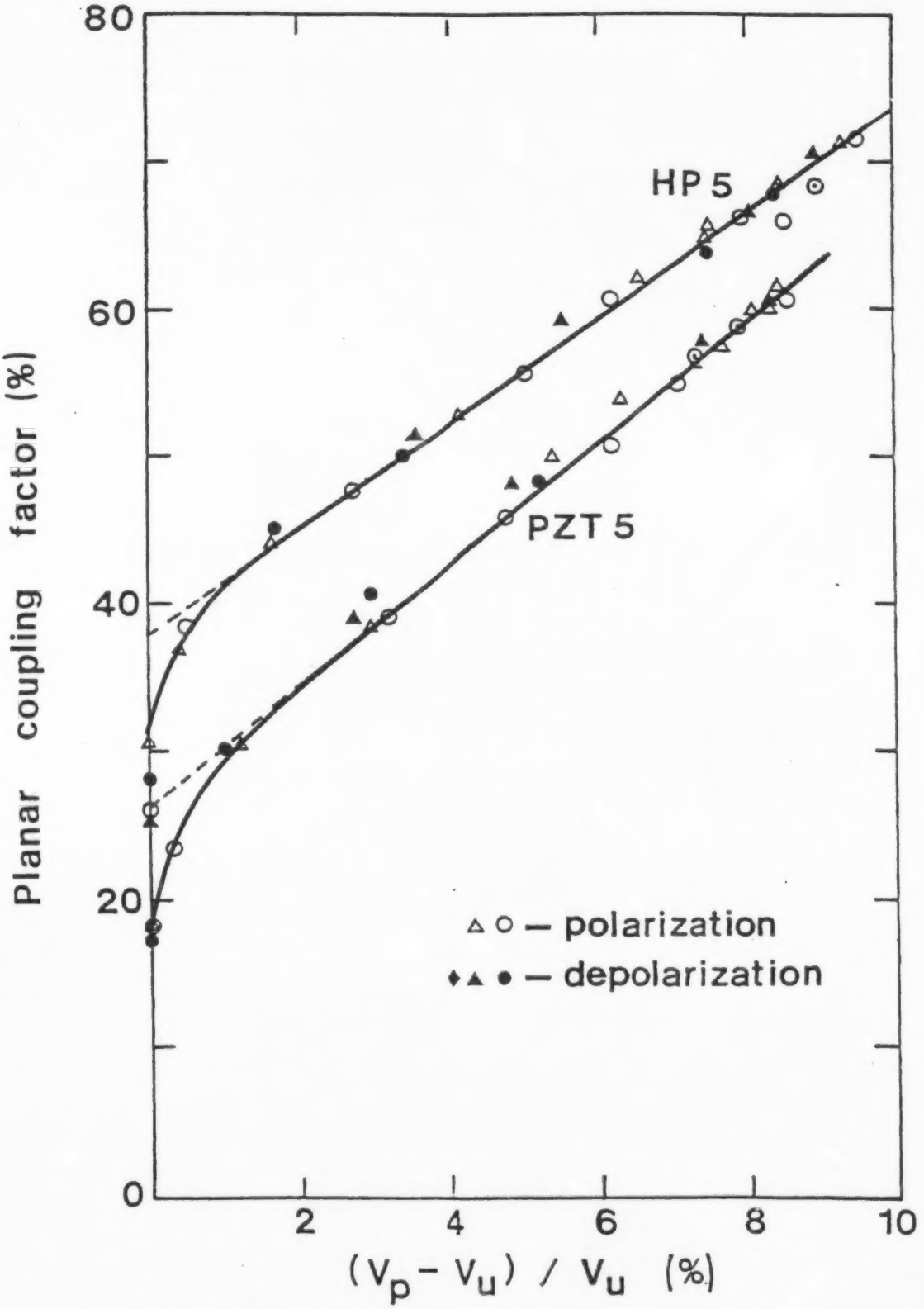

Figure 15: The variation of planar coupling coefficient with the change in compressional sound velocity measured in sintered PZT5 and hot-pressed HP5 at 50 MHz (V_p = velocity after polarization and V_u = velocity before polarization)

75 MHz PLANAR TRANSDUCER

Hot Pressed PZT4-B Material

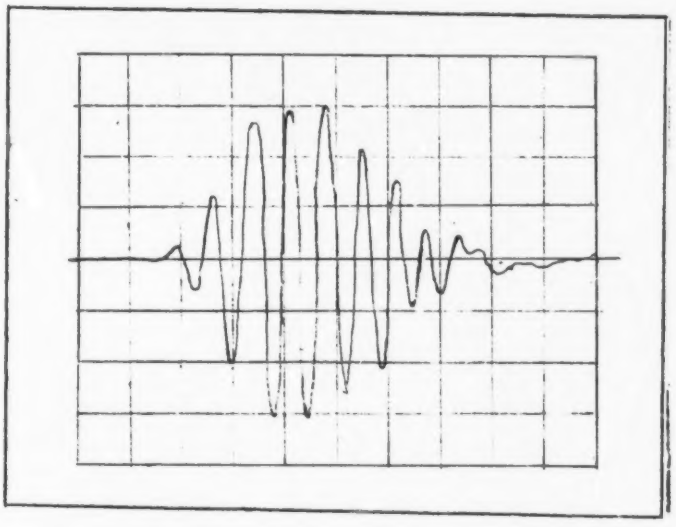

Figure 16(a)

2nd Backwall Reflection
From Steel Specimen
Hor 20 ns/div.
Vert 0.5 V/div.

Matec Tone Burst
Excitation

(picture refurbished)

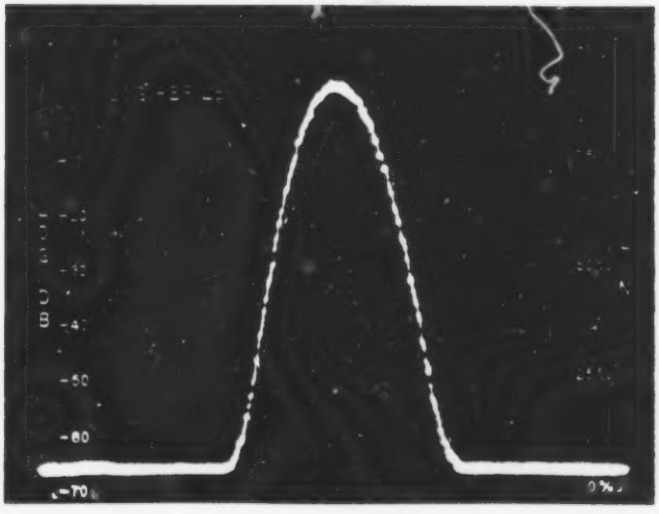

Figure 16(b)

Frequency Spectrum

Centre Freq.: 75 MHz
Hor 5MHz/div.

Atten: 34 dB

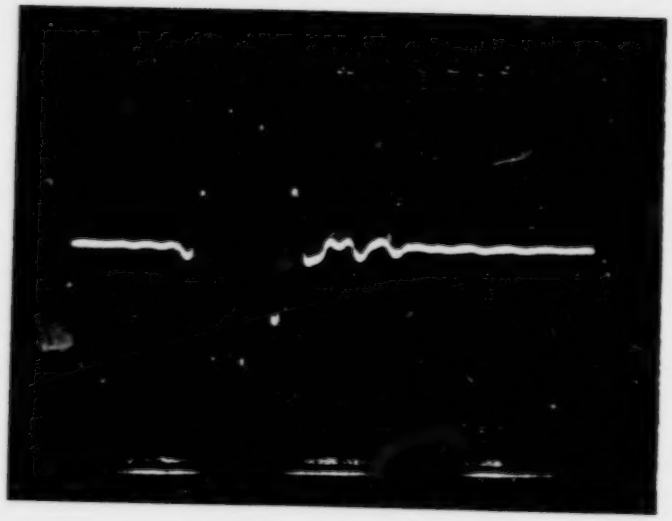

Figure 17(a)

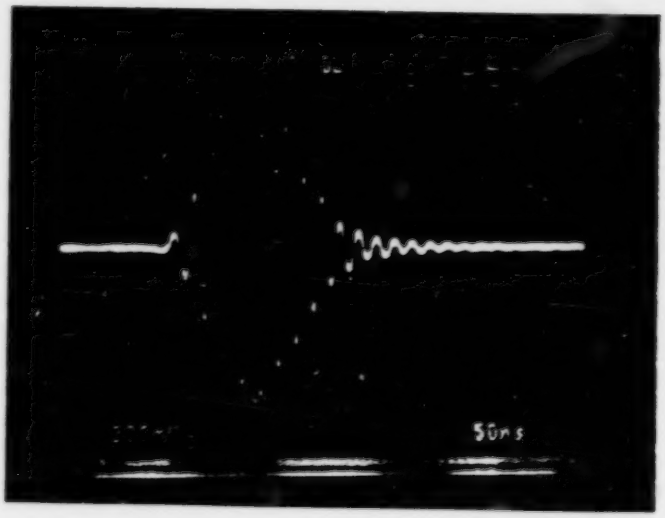

Figure 17(b)

Back reflected signals from glass plate immersed in water, using 36 MHz and 56 MHz focussed transducer, respectively. Transducers were excited with Matec tone burst system and attenuation level of 10 dB was used.

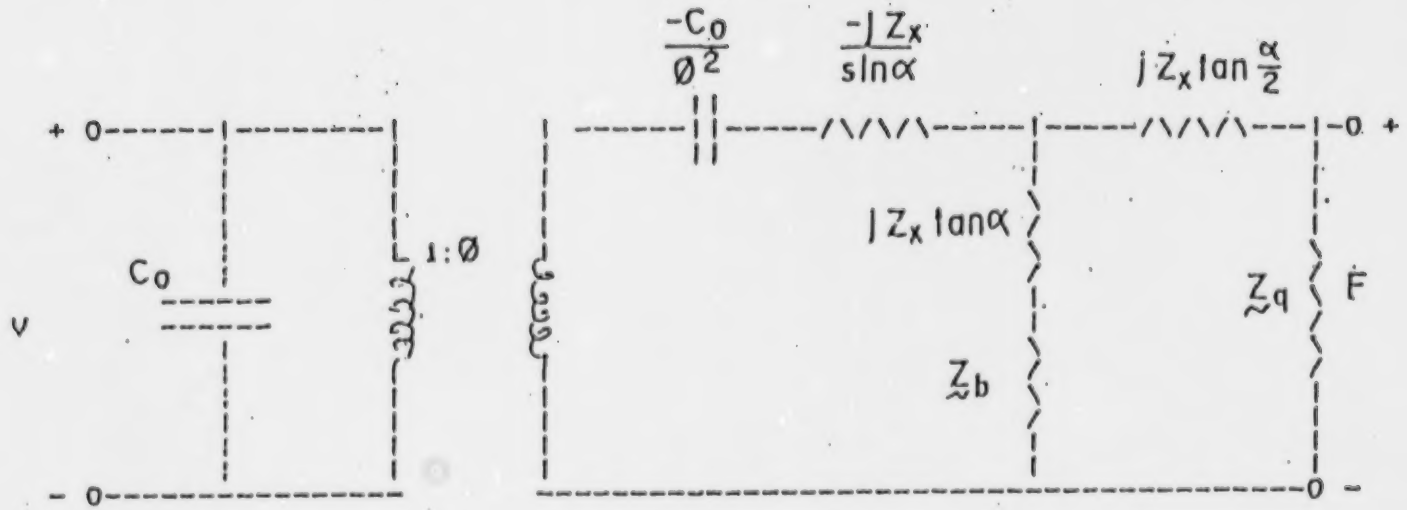

$K_q = \frac{Z_q}{Z_{mq}} : Z_{mq}$ → characteristic mechanical impedance of front matching section

$K_b = \frac{Z_b}{Z_{zb}} ; Z_{zb}$ → characteristic mechanical impedance of back matching section

Figure 18: General equivalent circuit for transducer loaded on both faces

C_o - clamped capacitance

Ø - ideal transformer ratio

Z_x - characteristic mechanical impedance of transducer

$\underset{\sim}{Z}_b$ - characteristic mechanical impedance of backing section

$\underset{\sim}{Z}_q$ - characteristic mechanical impedance of front section

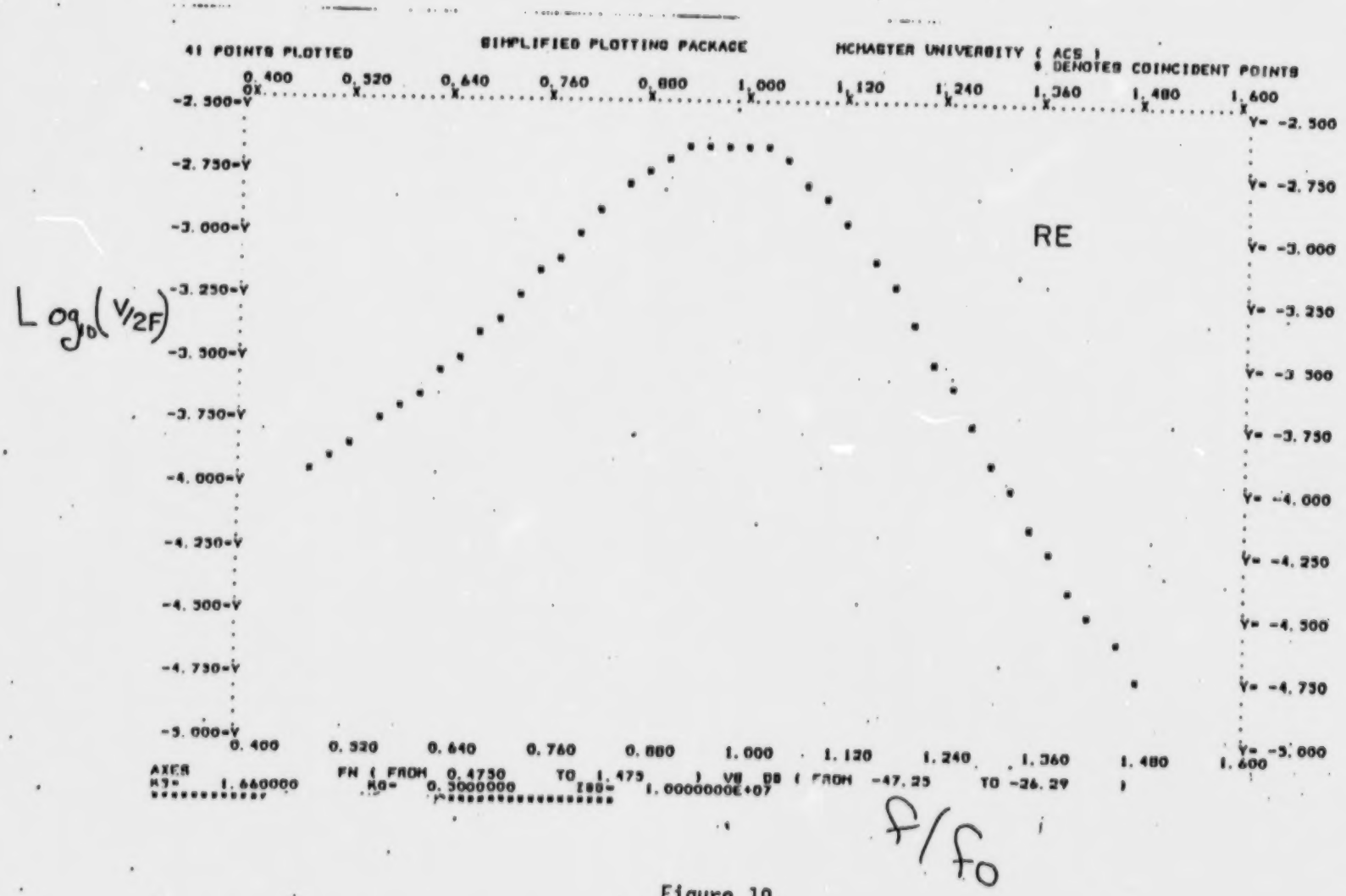

Figure 19

The dependence of the transfer function on a frequency deviation (f/f_o) for a receiving transducer using equivalent circuit of Fig. 18. Values for K_b, K_q, Z_b and Z_q are 1.66, 0.50, 1 x 10^6 g/cm^2.s and 0.15 x 10^6 g/cm^2.s, respectively.

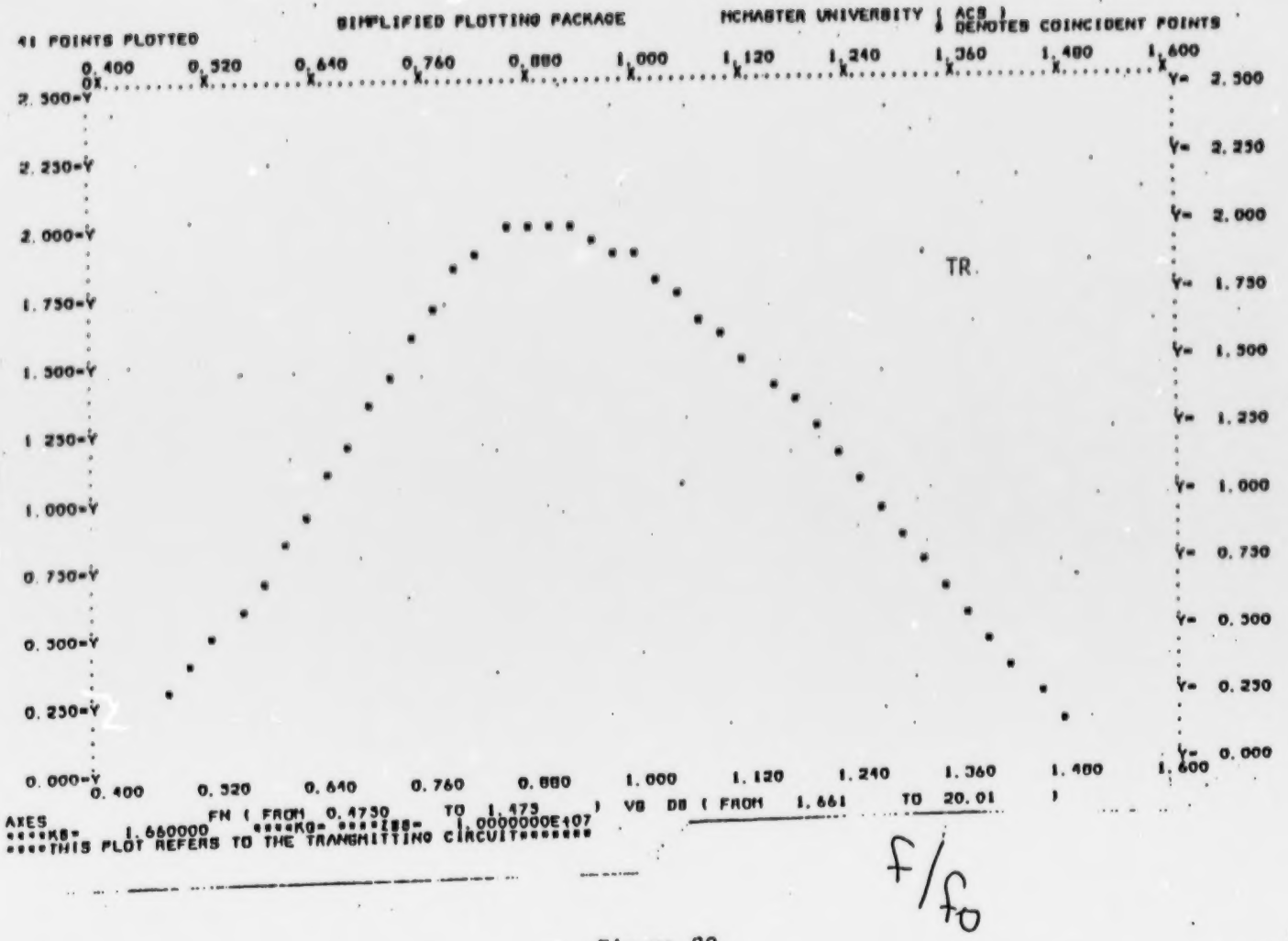

Figure 20

The dependence of the transfer function on a frequency deviation (f/f_0) for a transmitting transducer using equivalent circuit of Fig. 18. Values for K_b, K_q, Z_b and Z_q are 1.66, 0.50, 1×10^6 g/cm^2.s and 0.15×10^6 g/cm^2.s, respectively.

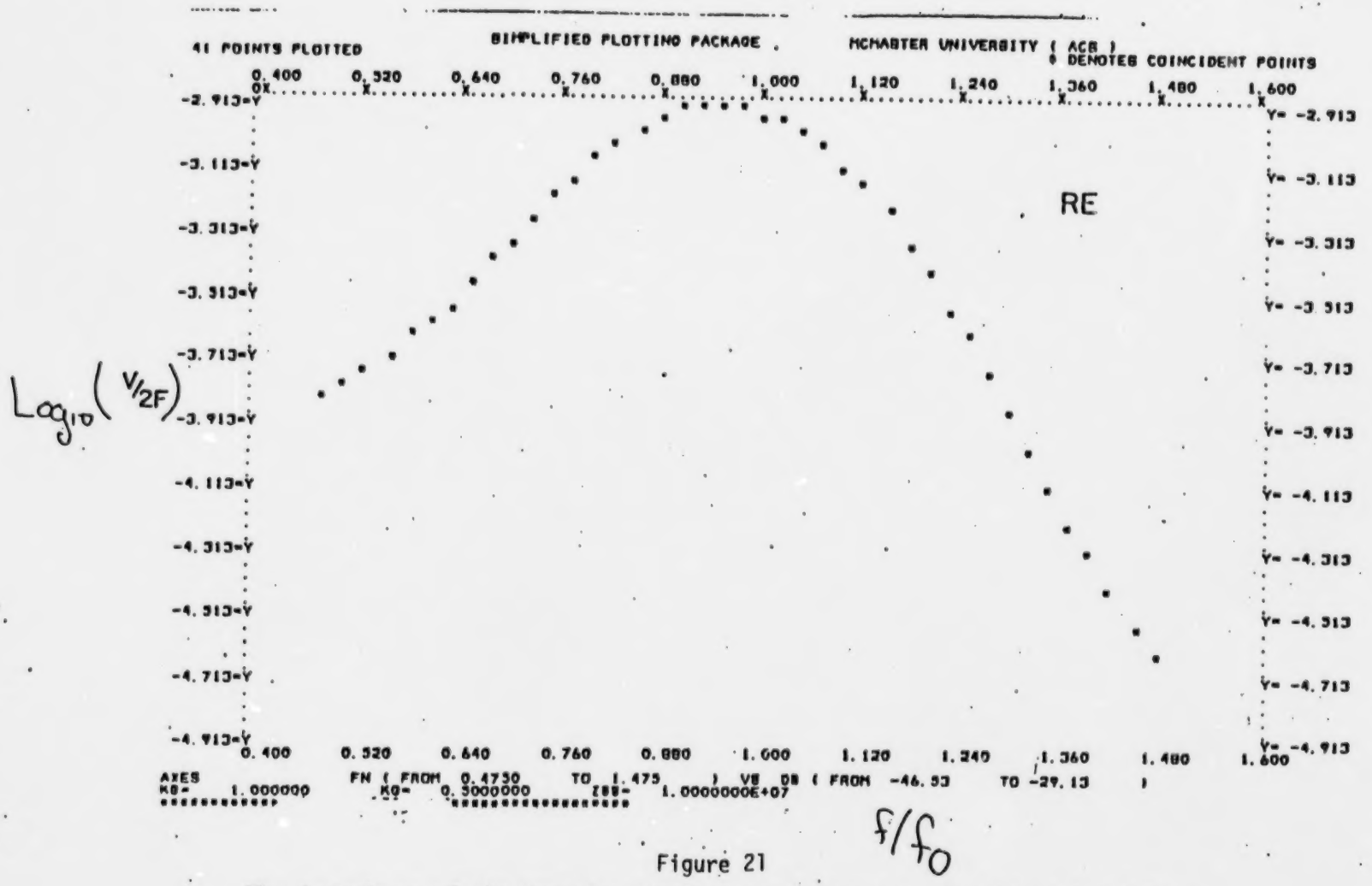

Figure 21

The dependence of the transfer function on a frequency deviation (f/f_0) for a receiving transducer using equivalent circuit of Fig. 18. Values for K_b, K_q, Z_b and Z_q are 1.00, 0.50, 1×10^6 g/cm^2.s and 0.15×10^6 g/cm^2.s, respectively.

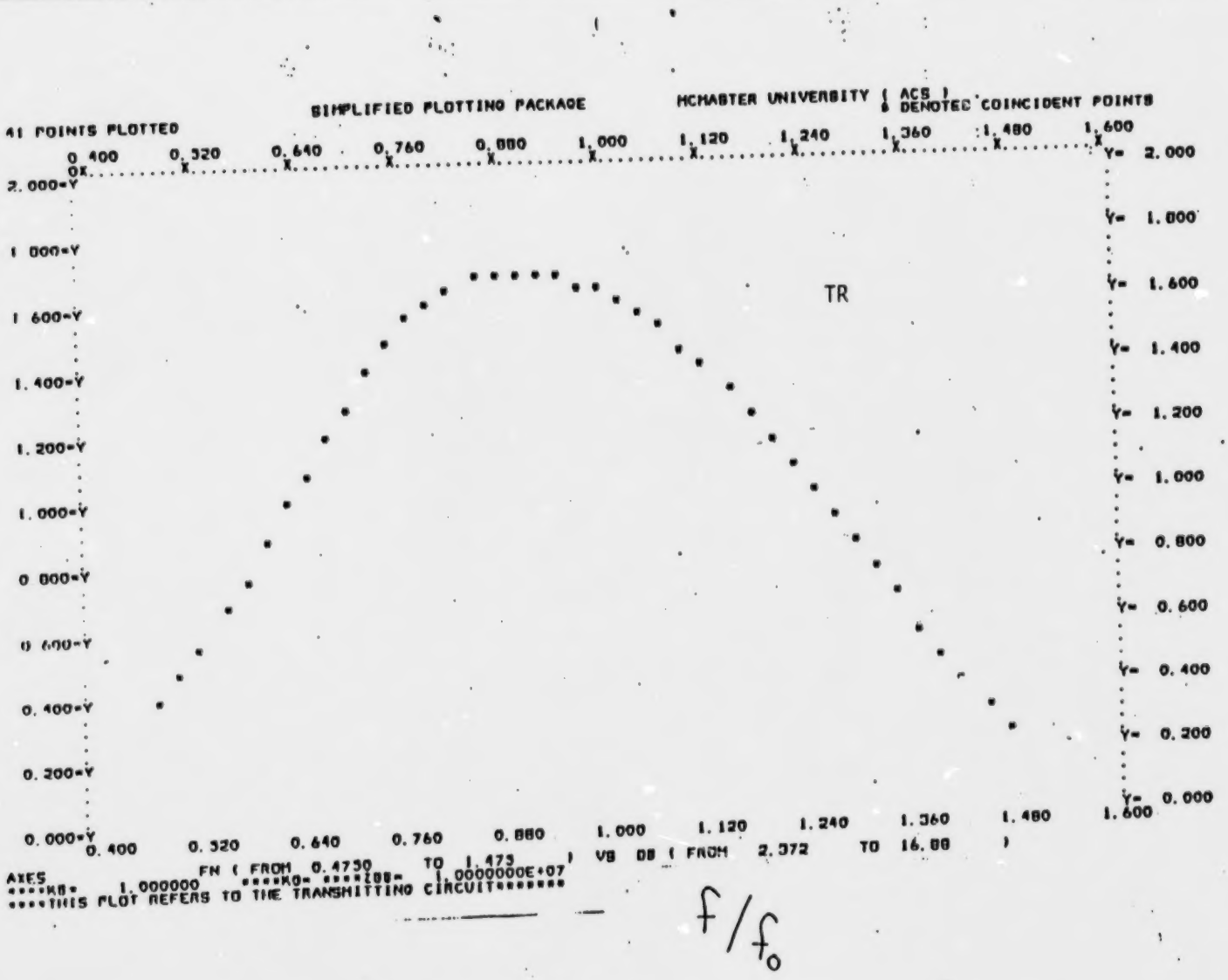

Figure 22

The dependence of the transfer function on a frequency deviation (f/f_o) for a transmitting transducer using equivalent circuit of Fig. 18. Values for K_b, K_q, Z_b and Z_q are 1.00, 0.50, 1 x 10^6 g/cm^2.s and 0.15 x 10^6 g/cm^2.s, respectively.

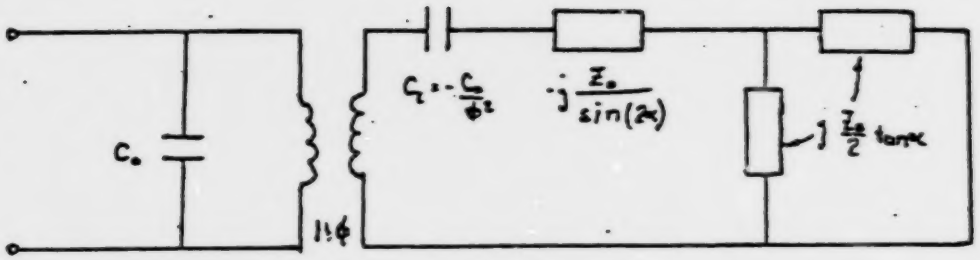

Figure 23

The general equivalent circuit for an undamped piezoelectric thickness resonator

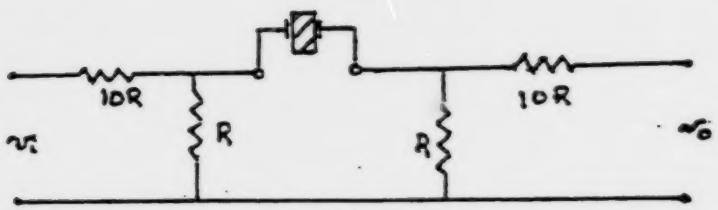

Figure 24

Circuit used to measure frequencies at maximum and minimum impedances

Parameter check:
Relative dielectric constant = 2100.00
Density (kg/mkk3) = 8010.00
Longitudinal Velocity (mm/microsec) = 4.860
Thickness (mm) = 0.0486
Electrode surface area (mmkk2) = 49.0000
Initial k value = 0.500 Final k value = 0.900
Initial frequency (MHz) = 25.000 Final frequency (MHz) = 175.000
Capacitance (farads) = 1.875E-08
Z0 (ohms) = 1.908E+03
Resonant frequency (Hz) = 5.000E+07
PHIkk2 /kkk2 = 3.576E+03
Maximum log10(Z) value = 0.2905
Minimum log10(Z) value = -3.4236
Angle of rotation (deg) = 45.00
Angle of tilt (deg) = 45.00
Number of frequency points (NX) = 52
Number of k points (NY) = 20

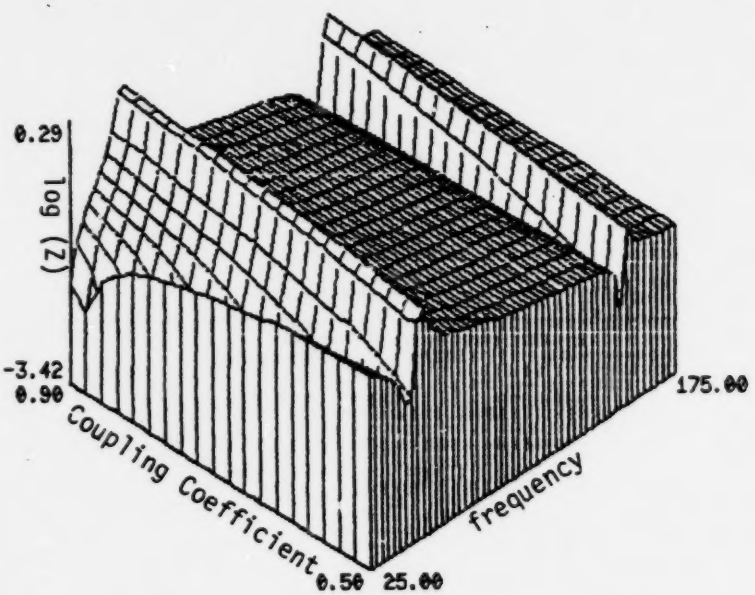

Figure 25

The plot of log |impedance| as a function of frequency and coupling coefficient using equivalent circuit of Fig. 23. It is clear from the graph that circuit resonance frequency shifts as coupling coefficient increases. Parameters used are tabulated above.

Parameter check:
Relative dielectric constant = 2100.00
Density (kg/mkk3) = 8010.00
Longitudinal Velocity (mm/microsec) = 4.860
Thickness (mm) = 0.0486
Electrode surface area (mmkk2) = 49.0000
Initial k value = 0.500 Final k value = 0.900
Initial frequency (MHz) = 25.000 Final frequency (MHz) = 175.000
Capacitance (farads) = 1.875E-08
Z0 (ohms) = 1.908E+03
Resonant frequency (Hz) = 5.000E+07
PHIkk2 /kkk2 = 3.576E+03
Maximum log10(Z) value = 0.2905
Minimum log10(Z) value = -3.4236
Angle of rotation (deg) = 10.00
Angle of tilt (deg) = 75.00
Number of frequency points (NX) = 52
Number of k points (NY) = 20

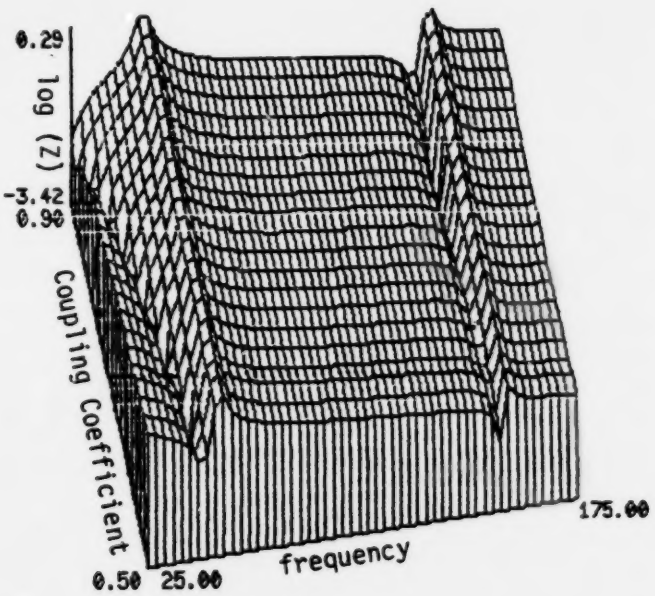

Figure 26

The plot of log |impedance| as a function of frequency and coupling coefficient using equivalent circuit of Fig. 23. It is clear from the graph that circuit resonance frequency shifts as coupling coefficient increases. Parametersused are tabulated above.

POOR

QUALITY

ORIGINAL